

Cyber-Physical Integration and Experimental Validation of Impeller Failures Using IoT-Enabled Digital Twin Framework

Thilak Sathish¹, Ronald Bardhoshi¹, Arivazhagan Anbalagan^{1,2}, Shone George², Marcos Kauffman²*

¹Faculty of Computing and Engineering, Priory Street, Coventry University, Coventry CV1 5FB, United Kingdom.

²The Institute for Advanced Manufacturing & Engineering, (AME), Beresford Avenue, Coventry University, CV6 5LZ, United Kingdom

Abstract. This interdisciplinary study investigates impeller failure using a combined digital and experimental approach, establishing a proof of concept for cyber-physical integration. First, a CAD model was developed and its structural integrity is validated using Finite Element Analysis (FEA) to ensure the impeller could withstand operational loads and dynamic stresses, following the methodology outlined in [1]. Next, an IoT-enabled digital twin framework was implemented with Arduino-based sensors (temperature, humidity, vibration) to monitor 3D-printed impellers made from 316L stainless steel and AlSi10Mg aluminium. The sensors were integrated with a custom test rig driven by a motor capable of 10,000 rpm, with data acquired via analog/digital interfaces and visualized in Node-RED, streaming in real time to an IoT cloud platform. Impeller experiments ran for over 80 hours and were tested under two corrosive conditions: (i) engine oil (5W-30) and (ii) saltwater. SEM/EDS analysis revealed carbon deposits on oil-exposed samples and aluminium oxide on saltwater-exposed ones, while further SEM imaging showed pitting and corrosion. Alicona surface roughness tests confirmed degradation under dynamic loads. Preliminary real-time monitoring demonstrated the of predictive maintenance alerts, though full-scale validation remains future work. Overall, the developed framework provides a robust basis for physical testing with digital representation, offering strong potential for predictive maintenance.

1 Introduction & Literature Review

In the rapidly evolving landscape of advanced manufacturing technologies, the convergence of Internet of Things (IoT), Digital Twins, and Artificial Intelligence (AI) is reshaping industrial operations and decision-making [2–4]. Digital Twins, serving as virtual representations of physical systems, enable real-time monitoring and predictive insights through IoT-enabled data acquisition [2,3]. This integration has transformed sectors such as

* Corresponding author: ad8181@coventry.ac.uk

hydrogen energy, where IoT and Digital Twins are increasingly applied to optimize production, compression, and transportation processes [4].

Within this technological paradigm, the impeller remains a critical component in fluid-handling systems. Its role in regulating flow dynamics, augmenting pressure, and ensuring operational efficiency is fundamental across vast applications. This includes centrifugal pumps, compressors, automotive cooling systems, aerospace, and hydrogen compression [5,6]. Despite its importance, research addressing impeller degradation mechanisms under cyber-physical monitoring frameworks remains limited. Understanding these mechanisms is essential for predictive maintenance and reliability in next-generation hydrogen and energy systems.

Research on impeller failures and corrosion phenomena has been extensive. Investigation has been conducted on erosion-corrosion damage in water-pump impellers [5]. The study observed that prolonged exposure (~ 6 months) significantly reduced pumping efficiency in cooling systems. Using powered microscopy and precise weight measurements, surface degradation characterized by pits and rust was confirmed, which intensified corrosion over time. Similarly, failure analysis of an MVR impeller operating in a dairy processing plant has been reported [7]. The impeller blade fracture occurred after 150 hours of service, and scanning electron microscopy revealed that torsional stress-induced vibration was the primary cause, accelerating fatigue failure. Further examination of locomotive draught fan impellers identified welding defects such as cavities and porosities as critical factors leading to blade breakage [8]. Susceptibility of FV520B to sulphide stress corrosion cracking (SSCC) has also been studied using constant displacement loading tests and finite element analysis (FEA) [9]. Findings indicated that high hydrogen sulphide concentrations combined with stress concentration around corrosion pits significantly increased SSCC risk. Additionally, fatigue failure in semi-open impeller blades has been investigated through numerical and experimental approaches [10]. Mistuning phenomena, elevated stress, and increased natural frequencies were found to collectively reduce fatigue life.

Beyond mechanical failures, emerging technologies are fundamentally transforming industrial operations. Big data analytics has become a cornerstone of Industry 4.0, enabling advanced pattern recognition, predictive insights, and real-time process optimization [11]. Its ability to process massive datasets allows manufacturers to anticipate equipment failures, optimize resource allocation, and streamline production workflows. Studies have highlighted how big data facilitates automation, reduces reliance on human intervention, and supports adaptive decision-making [12–14]. Frameworks using big data for efficient load balancing and seamless communication between cloud systems and shop floor operations have been proposed [13]. Industrial wireless sensor networks play a critical role in enabling real-time data acquisition and control [14]. In recent years, digital twin technologies have emerged as a key enabler of cyber-physical integration. Defined as real-time software representations of physical systems, they facilitate optimization and predictive analytics [15]. Reported benefits include cost reductions of up to 30%, planning time savings of 20%, and productivity improvements of 8% [16]. Further research emphasizes the integration of digital twins and cyber-physical systems for smart manufacturing and system-level simulation [17,18]. Parallely, IoT technologies continue to revolutionize production systems. IoT enhances production quality and minimizes downtime through factory digitization and intelligent data management [19]. IoT-based approaches for dynamic resource management in smart factories reinforce the growing importance of connected systems in achieving operational efficiency [20].

Complementing these technologies, blockchain integrated with edge computing addresses Industry 5.0 challenges such as decentralization, security, and scalability [21]. Blockchain ensures data integrity through consensus mechanisms like PoW, PoS, and dPoSec, while edge computing reduces latency and supports real-time decision-making at

the network edge. Furthermore, industrial communication protocols are evolving to meet interoperability demands. Comparative studies on OPC UA and MQTT within a Unified Namespace (UNS) aligned with RAMI 4.0 reveal that OPC UA offers robust semantic modeling and security, whereas MQTT excels in lightweight, high-frequency data transmission [22, 23]. Both studies conclude that hybrid architectures combining these protocols can deliver scalable, interoperable solutions for smart manufacturing ecosystems, paving the way for fully integrated digital factories. Despite extensive research on impeller failures and digital manufacturing technologies, few studies have integrated real-time sensor data with simulation models for predictive maintenance. Compared to traditional monitoring approaches that rely on periodic inspections, the proposed IoT-enabled digital twin framework offers continuous data acquisition and real-time anomaly detection, addressing multifaceted challenges in impeller performance while significantly improving reliability and reducing unplanned downtime.

2 Methodology

This study adopts a cyber-physical approach to assess impeller performance and failure mechanisms. Impellers were 3D-printed using materials validated through Finite Element Analysis (FEA) and tested under controlled conditions. Real-time sensor data temperature, humidity, and vibration was captured via Arduino-based systems and visualized in Node-RED [24] using C++ and JavaScript, with continuous streaming to an IoT cloud platform. This enabled the creation of a digital twin for predictive maintenance and simulation validation. The methodology is presented in sequential stages: (i) cyber-physical system setup, (ii) FEA simulations, (iii) experimental procedures validated through Scanning Electron Microscopy (SEM) and Energy Dispersive X-ray Spectroscopy (EDS) which identifies elemental composition to assess corrosion and material degradation and (iv) Surface roughness measurements.

2.1 IoT Setup and Digital Twin Methodology

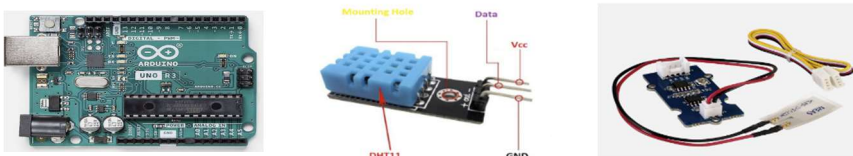


Fig.1. Proposed IoT-based architecture using Arduino UNO R3, integrated with Node-RED

Fig.1 illustrates the proposed IoT-based architecture using Arduino UNO R3 [25] (Fig.2(a), integrated with Node-RED for real-time sensor control and data streaming to a cloud platform Insights Hub [26]. The system connects via USB to a PC or laptop, enabling live monitoring of temperature, humidity, and vibration sensors. This setup offers a low-cost, open-source solution for industrial failure analysis with minimal resource requirements [2]. Fig.2 (b)-(c) show the DHT11 (temperature & humidity) and Piezo vibration sensors used for data acquisition in this study. In this setup, sensors are connected to the Arduino UNO following standard procedures [25, 27]. These connections allow the Arduino to read environmental and mechanical data in real time, which is then processed and visualized through Node-RED. Once the circuit is configured, a C++ program is uploaded via the Arduino IDE (Fig.3(a)) to activate sensor readings and transmit data through the serial port. On the software side, Node-RED (Fig. 3(b)) is used to create a flow that reads serial data from the Arduino, processes it using JavaScript functions (function 7), and visualizes it through dashboard nodes. Fig. 3 (b) illustrate the flow configuration, function node code,

serial port setup, and dashboard interface (Fig 4(a)), demonstrating how sensor data is captured, processed, and displayed for engineering insights and predictive diagnostics. Here debug (debug14) node help monitor data integrity and detect errors, while ‘mind connect’ node allow data sent to a cloud platform Insights hub for remote access and further analysis.

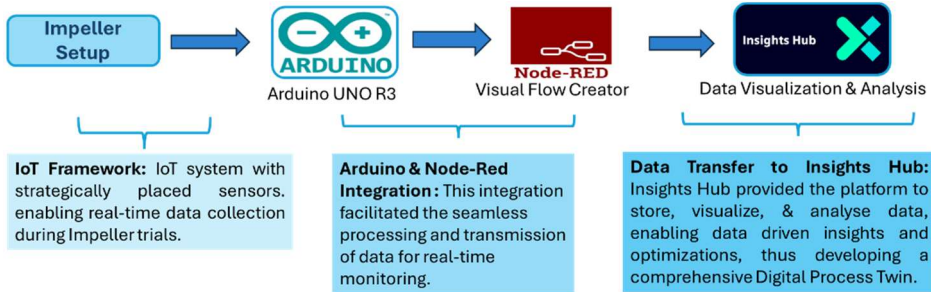


Fig.2. (a) Arduino UNO R3 (b) DHT11- Temperature & Humidity Sensor (c) Piezo Vibrating Sensor

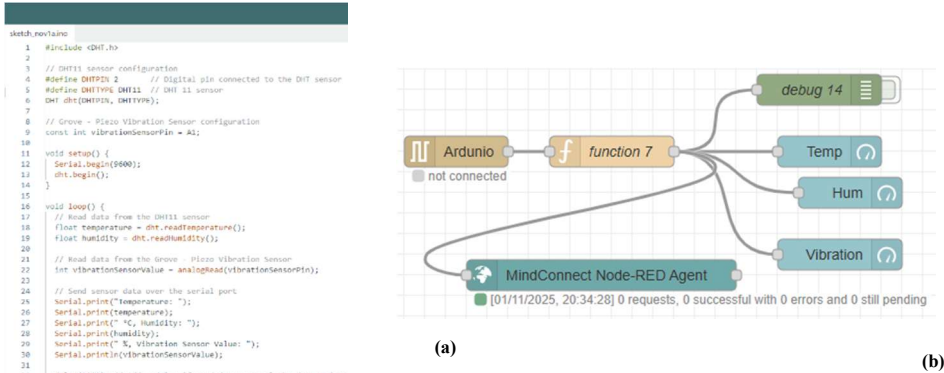


Fig. 3 (a) Arduino IDE (b) Node-Red Flow

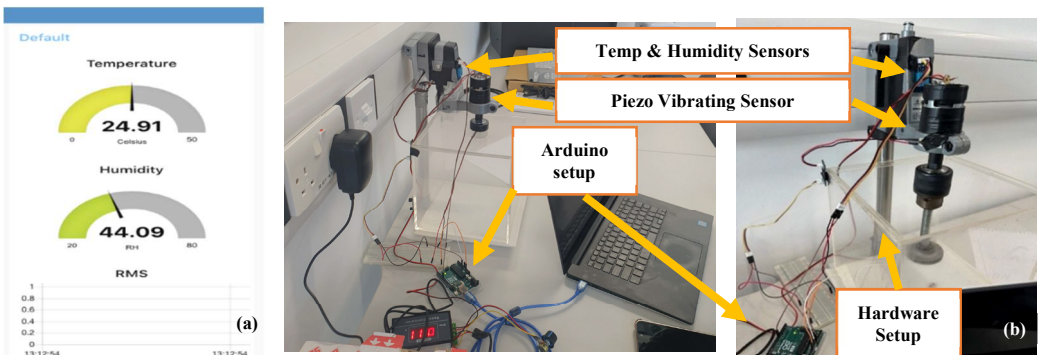


Fig. 4. (a) Dashboard interface (b) Hardware setup with IoT connection

The digital twin component in this work extends beyond monitoring and visualization by incorporating predictive logic and degradation-aware mechanisms through IoT-based rule settings. Temperature, Humidity and Vibration data from the impeller is continuously streamed to Siemens Insights Hub, where an asset representing the impeller is created and linked to real-time sensor signals. Figure 5(a) shows the asset created in Insights Hub, while Figure 5(b) illustrates the rule configuration for vibration monitoring. In addition to vibration, environmental parameters such as temperature and humidity are captured and displayed

alongside the vibration signals, as shown in Figure 5(c). Based on these inputs, three rule settings were created to monitor critical vibration thresholds and environmental conditions, enabling automated actions when abnormal patterns often indicative of imbalance or material degradation are detected. When the vibration exceeds the predefined limits, an email notification is triggered and sent to the user, as shown in Figure 5(d). This closed-loop mechanism ensures timely intervention and links high vibration events to potential degradation mechanisms, allowing the digital twin to dynamically update, predict failures, and support proactive maintenance within a cyber-physical workflow.

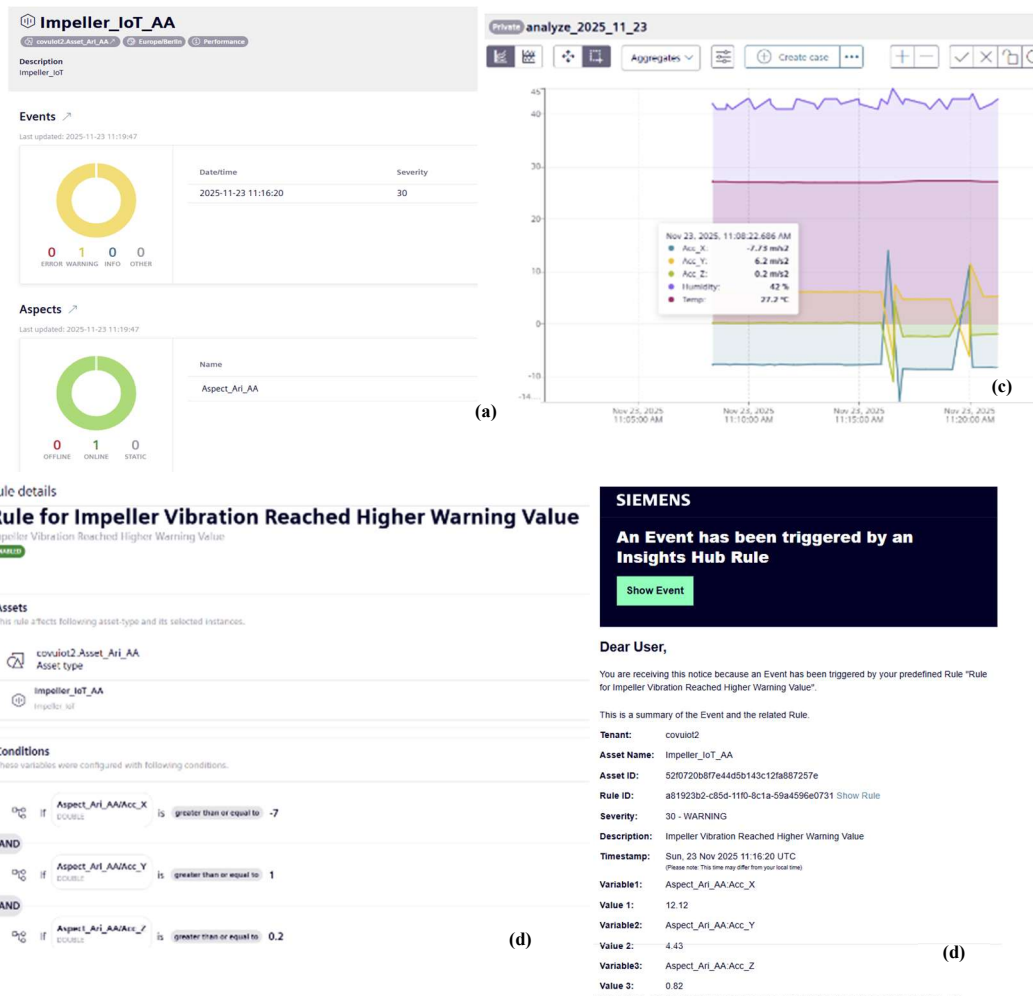


Fig. 5. (a) Asset created in Siemens Insights Hub for impeller vibration monitoring (b) Rule configuration in Insights Hub for vibration threshold detection (c) Real-time vibration signals displayed along with temperature and humidity data (d) Email notification triggered automatically when vibration exceeds the set threshold.

Fig. 4(b) shows the hardware setup with IoT connectivity during testing. Tests were conducted at machine speeds of 1000, 3000, 4000, and 5000 rpm to observe sensor responses and machine behavior. Table 1 summarizes sensor data across these speeds, showing gradual increases in temperature and vibration, and a slight drop in humidity. Vibration spiked sharply at 4000 rpm, indicating possible fatigue or misalignment. At 5000 rpm, vibration exceeded 1000 mm/s RMS, suggesting a critical threshold. These results highlight the value

of integrating edge technologies with conventional machinery for real-time diagnostics and predictive maintenance via cloud-based monitoring.

Table 1 Comparative summary of sensor data across the speed levels

RPM	Temperature (°C)	Humidity (%)	Vibration (mm/s RMS)
1000	22.00	55.00	19
3000	22.50	54.00	24
4000	22.60	51.00	1009
5000 Rpm			
5000	22.60	51.00	1007
5000	22.60	51.00	1009
5000	22.60	51.00	1010
5000	22.50	51.00	1022

3 CAD Modelling, FEA Analysis & 3D printing

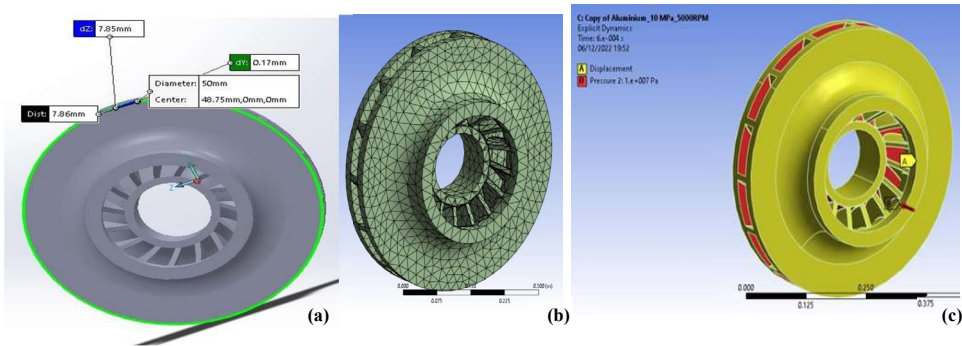


Fig. 6. (a) CAD Models (b) Meshing in Ansys (c) FEA Setup

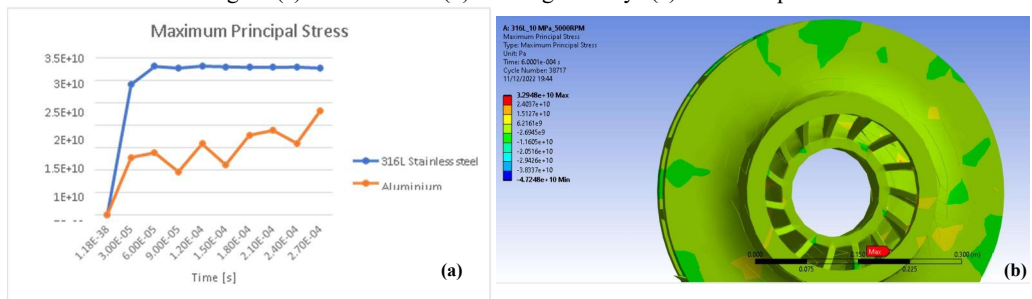


Fig.7. (a) Maximum Principal Stress (b) FEA visualization of the SS impeller at 5000 RPM

The impeller design process began with CAD modeling in SolidWorks, scaling down original diameter of 500 mm to 50 mm (1:10 ratio) (Fig. 6(a)). This is for experimental feasibility while maintaining geometric integrity. This scaled model is used to evaluate structural performance under operational conditions, Finite Element Analysis (FEA) was conducted using ANSYS Explicit Dynamics for both AlSi10Mg aluminum alloy and 316L stainless steel impellers [1]. Meshing (Fig. 6(b)) was performed and simulation setup incorporated displacement support, constant pressure load, and rotational velocity to replicate real-world stresses (Fig 6(c)). Fig. 7(a) illustrates the variation of maximum principal stress over time for impellers made of 316L stainless steel and AlSi10Mg aluminum alloy under a rotational

speed of 5000 RPM. The SS impeller exhibits a rapid increase in stress, stabilizing at approximately 3.2×10^{10} MPa, indicating its higher stiffness and resistance to deformation under dynamic loading. In contrast, the aluminum impeller shows a more gradual and fluctuating stress response, reaching a peak of around 2.0×10^{10} MPa. These differences highlight the influence of material properties such as Young’s modulus and density on structural performance under high-speed rotation. The results confirm that stainless steel offers superior strength, while aluminum demonstrates lower stress levels but with more variability, which may affect fatigue life under prolonged operation. Fig. 7(b) shows the FEA visualization of the stainless-steel impeller at 5000 RPM, highlighting stress distribution. The analysis provided valuable insights into deformation and stress distribution under combined rotational and aerodynamic loads. Finally, after FEA simulation, the validated designs were 3D printed (Fig. 8(a) & (b)), using Selective Laser Melting (SLM) technology for both materials. This integrated approach combining modeling, simulation, and additive manufacturing ensured accurate performance assessment and supported the development of a digital twin for predictive maintenance.

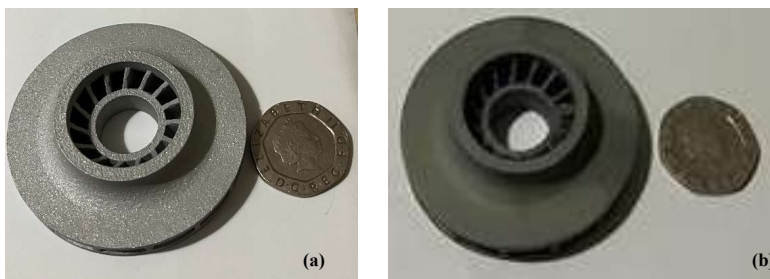


Fig. 8. Impeller (a) (Alsi10mg) Aluminium (b) 316L stainless steel

4 Experimental Setup and Pre-Characterization

Table 2: Chemical Properties of Working Mediums

Property	Engine Oil (5W-30)	Saltwater
Specific Gravity (15°C)	0.859	~1.025
Kinematic Viscosity (40°C)	71.5 mm ² /s	N/A
Viscosity Index	160	N/A
Flash Point	195°C	N/A
Pour Point	-38°C	N/A
Salt Concentration	N/A	35 g/L

The experiments were conducted in two different mediums engine oil (5W-30) and saltwater under both static and dynamic conditions involving impeller rotation at 5000 RPM. To ensure reliability, pre-experimental characterization was performed using a Zeiss Gemini Sigma Scanning Electron Microscope (SEM). SEM imaging provided detailed surface morphology, while surface roughness measured using an Alicona optical 3D microscope, reported parameters such as Ra, Rq, and Rz. These analyses ensured accurate baseline data before immersion tests. Following this, the impellers were immersed in the selected mediums for corrosion and wear evaluation. In engine oil and saltwater, the AlSi10Mg impeller and 316L stainless steel impeller remained for greater than 80 hours. The chemical properties of the working mediums are summarized in Table 2.

5 Results and Discussions

5.1 Experiment Comparison - Baseline, Before Experiment

Prior to exposure, the aluminium (AlSi10Mg) impeller’s top surface was examined using SEM, and elemental composition was obtained via EDS at the highlighted point (Fig. 9). The corresponding spectrum confirms the expected alloy constituents, with aluminium as the major element (68.5%), followed by oxygen (24.6%), silicon (4.5%), and minor additions of silver (2.0%) and magnesium (0.3%). The high oxygen content indicates a native oxide film, contributing to corrosion resistance, while traces of silver and magnesium likely originate from alloying or residual additives that enhance strength and stability.

Similarly, the 316L impeller was characterized using SEM/EDS before testing. Fig. 10 shows the SEM field and EDS spectrum from the top surface, revealing iron as the dominant element (51.8%), along with oxygen (16.9%), chromium (13.8%), nickel (7.9%), and molybdenum (2.1%), with traces of manganese and silicon. Elevated oxygen suggests surface oxidation typical of stainless steel, which improves corrosion resistance. Chromium and molybdenum enhance pitting resistance, while nickel contributes to toughness and stability. Minor elements such as manganese and silicon originate from alloying additions that support strength and microstructural integrity.

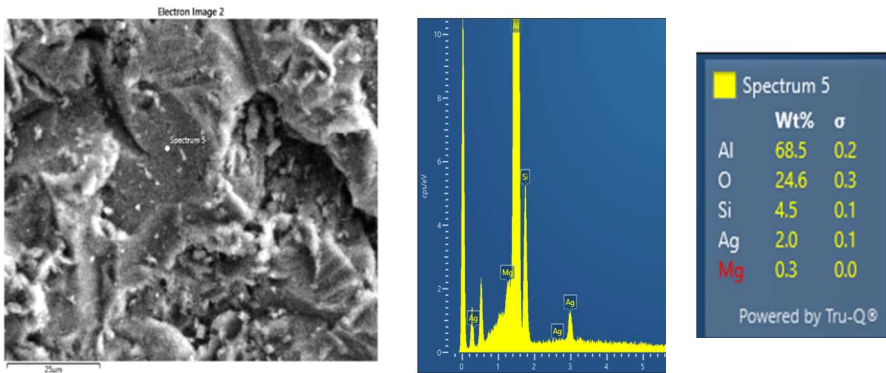


Fig. 9. SEM and EDS image of aluminium impeller before experiment

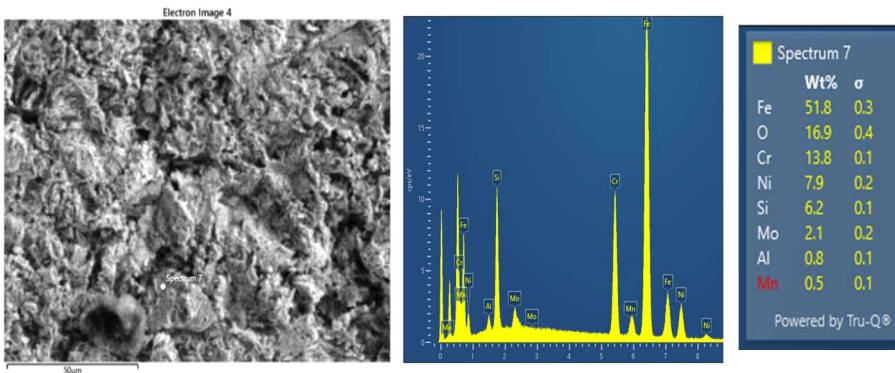


Fig.10. SEM and EDS image of 316L impeller before experiment

5.2 Experiment Comparison - Impeller in Oil Medium (Post-Exposure)

After oil exposure, SEM/EDS analysis of the aluminium impeller confirms significant surface chemistry changes and carbon-rich deposits. Representative micrographs and spectra are shown in Fig. 11. The EDS results indicate a marked increase in carbon (80.8%), along with aluminium (55.7%) and oxygen (49.9%), while silicon remains minimal (0.6%). This composition suggests heavy carbon contamination from the oil medium, combined with residual aluminium and oxide layers from the base alloy, indicating strong chemical interaction at the surface. Similarly, Fig. 12 illustrates the surface morphology of the 316L stainless steel impeller post oil exposure, revealing a rough, uneven texture with visible deposits. The corresponding EDS spectrum confirms substantial carbon contamination (124.8%), along with minor oxygen (5.4%), iron (4.3%), and alloying elements such as chromium (1.5%), zinc (1.0%), and traces of silicon and phosphorus. The elevated carbon concentration indicates significant deposition from the oil medium, while reduced iron and chromium signals suggest masking of the base alloy by surface films. These findings highlight strong interactions between the oil’s hydrocarbon structure and the impeller surface during prolonged immersion, leading to surface modification and potential performance degradation.

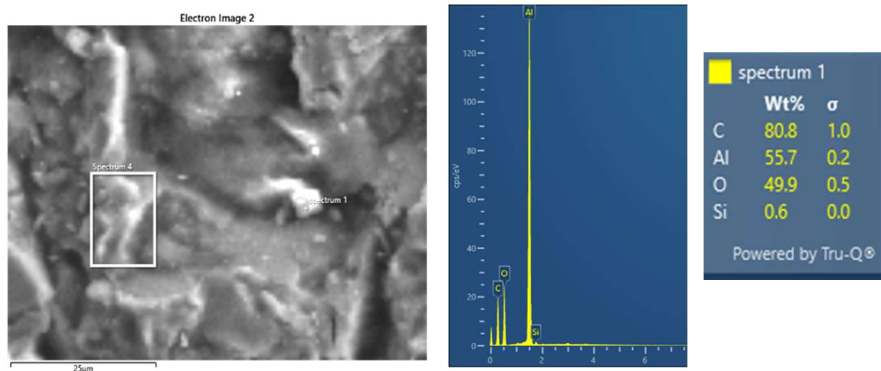


Fig.11. SEM and EDS image of aluminium impeller after experiment in oil medium

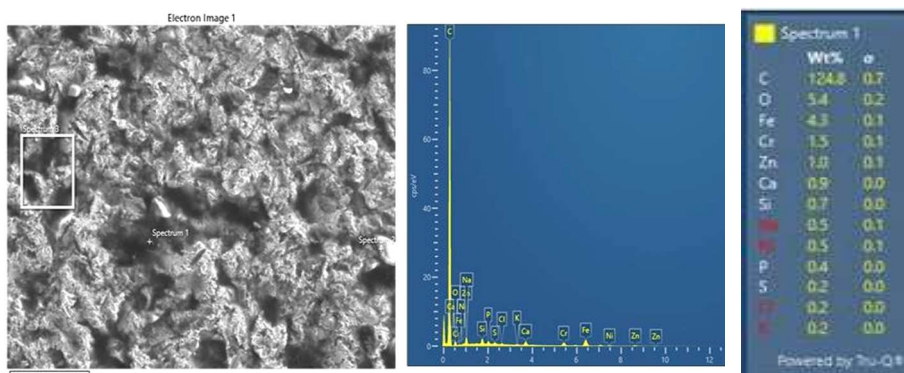


Fig. 12. SEM and EDS image of 316L impeller after experiment in oil medium

5.3 Experiment Comparison - Impeller in Saltwater Medium (Post-Exposure)

The SEM/EDS image (Fig.13) on the left shows the surface morphology of the aluminium impeller after prolonged exposure to saltwater, revealing rough, uneven regions with distinct deposits. The EDS spectrum in the center and the composition table on the right indicate a

high presence of oxygen (30.7%), followed by aluminium (16.5%), along with carbon (5.2%) and chlorine (4.3%), with traces of zinc and sulphur. The elevated oxygen content suggests significant oxide formation, while chlorine indicates aggressive saltwater corrosion. These findings confirm that aluminium reacts strongly in chloride-rich environments, forming aluminium oxide (Al_2O_3) and localized corrosion sites, which compromise surface integrity.

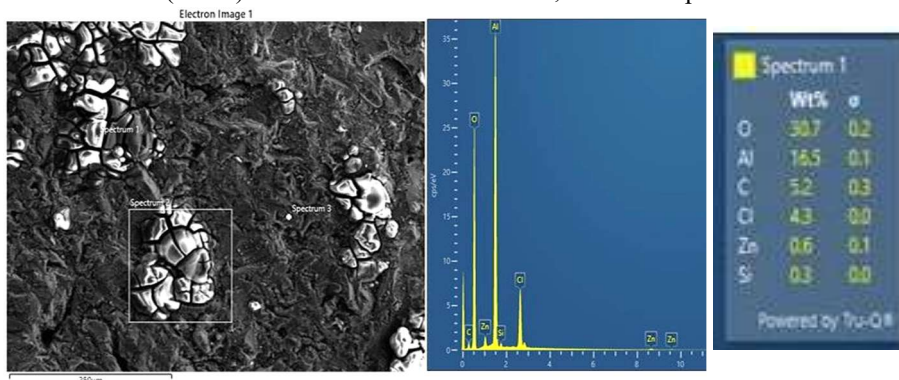


Fig.13. SEM and EDS image of aluminium impeller after saltwater exposure

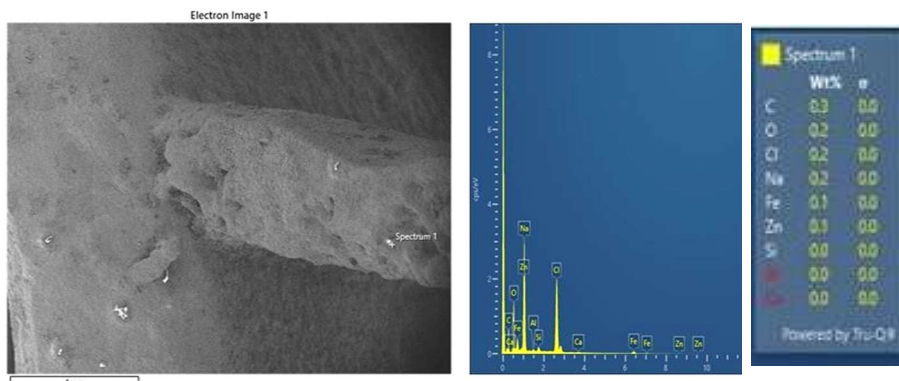


Fig. 14. SEM and EDS image of 316L impeller after saltwater exposure

EDS analysis of 316L stainless steel (Fig.14) after saltwater exposure shows Cl (0.2%), Fe (0.7%), O (0.2%), Zn (0.1%), and C (0.3%). Even though 316LSS contains high chromium and nickel for corrosion resistance, chloride ions from salt water can penetrate and locally break down the passive film, initiating pitting corrosion. Oxygen indicates oxide interaction, while Fe and C are from the base alloy. Trace Zn may be from contamination. This confirms early chloride-induced attack despite the alloy's inherent resistance. These findings confirm that aluminium reacts strongly in chloride-rich environments, forming aluminium oxide (Al_2O_3) and localized corrosion sites, which compromise surface integrity.

Fig. 15 shows SEM images of aluminium and 316L impellers under three conditions: (a) baseline, (b) after oil exposure, and (c) after saltwater exposure. Although surface changes are subtle and difficult to identify visually, the highlighted regions in the SEM figures indicate areas where defects such as micro cracks, pitting corrosion, or crevices are present. EDS analysis confirms chemical changes, including chloride presence after saltwater exposure, signalling passive film breakdown and early corrosion. This demonstrates the need to combine SEM with EDS for accurate degradation assessment.

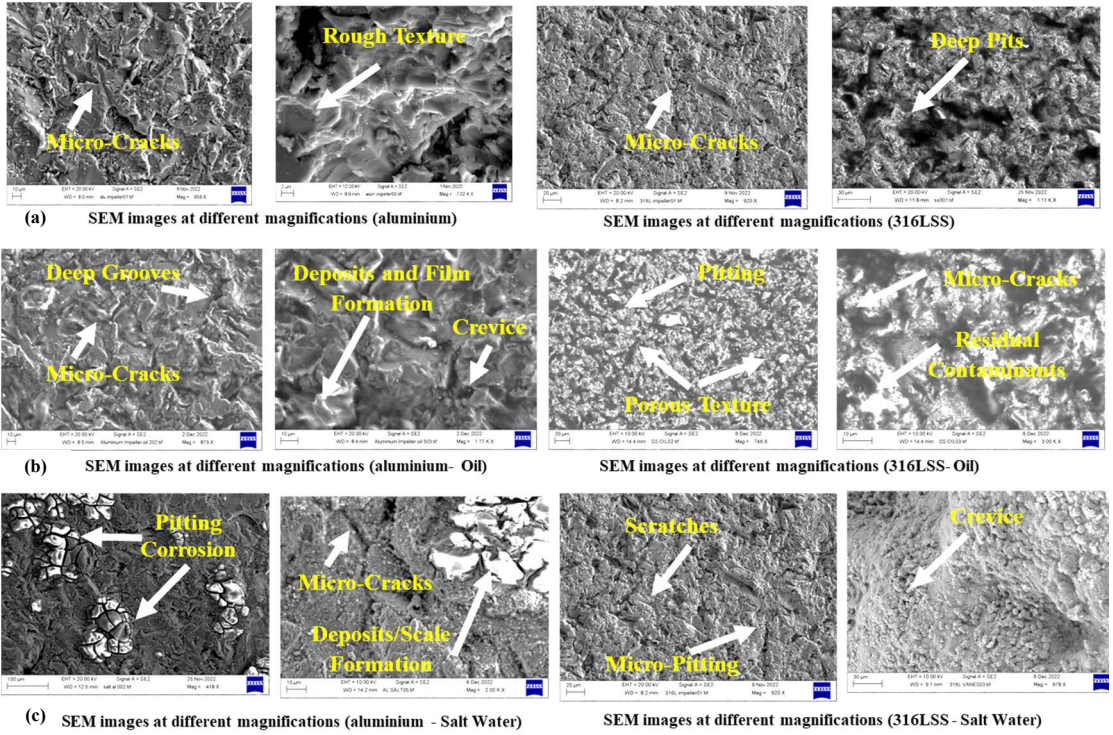


Fig. 15. SEM images of aluminium and 316L impeller (a) baselines (b) Oil medium exposure (c) saltwater exposure

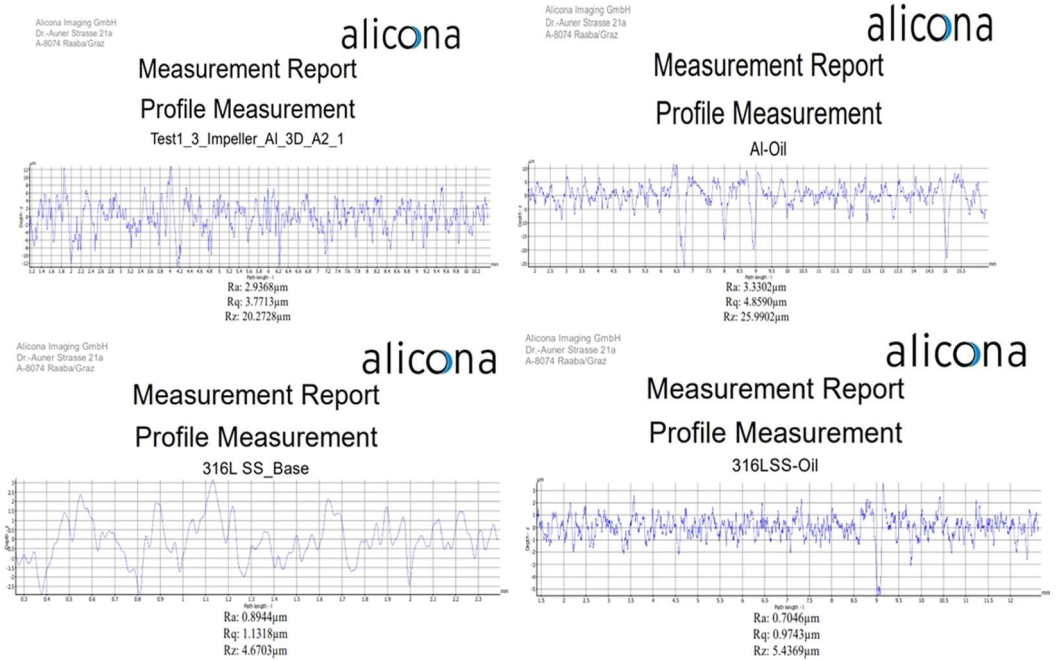


Fig.16. Alicona measurement for Aluminium and 316LSS before and after experiment

6 Surface roughness Measurement with Alicona

Surface roughness was measured using an Infinite Focus Microscope (Alicona), an optical 3D system with lateral resolution down to 400 nm and vertical resolution of 10 nm. Profile parameters were set at width = 100 (profile) and 105.1942 μm (metric), applying roughness filtering per ISO 4287 and ISO 4288. Impeller surfaces were examined before and after tests in oil and saltwater using aluminium and 316L stainless steel. *Due to page limits, detailed profiles are shown only in Fig. 16 for aluminium and 316L impellers before and after oil exposure.* In oil, aluminium roughness increased from $R_a = 2.93 \mu\text{m}$ to $3.30 \mu\text{m}$ due to abrasive wear from particle-laden oil acting on its softer surface. In contrast, 316L roughness decreased from $R_a = 0.89 \mu\text{m}$ to $0.70 \mu\text{m}$ as lubrication and hardness produced a polishing effect. In saltwater, aluminium roughness dropped from $2.93 \mu\text{m}$ to $2.46 \mu\text{m}$, likely from oxide formation and removal of asperities, while 316L decreased from $0.89 \mu\text{m}$ to $0.72 \mu\text{m}$ due to passive film stability and hydrodynamic polishing. These results reflect the combined influence of material properties, lubrication, corrosion, and operating conditions on surface integrity.

7 Conclusions

This study demonstrates the potential of digital twin technology for IoT-enabled impeller failure diagnosis, offering a foundation for predictive maintenance and performance optimisation. This integrated approach enhances reliability by enabling early failure detection and reducing downtime compared to conventional reactive monitoring methods. To achieve this, two 3D-printed impellers - 316L SS and AlSi10Mg were tested in oil and salt-water media, with before/after comparisons supported by microstructural analysis, surface roughness evaluation, and explicit dynamics simulation at 5000 rpm to identify stress distribution, deformation, and strain. Key findings include colour changes on aluminium in oil (silver to grey) due to chemical interaction, pore formation from carbonaceous elements, scratches on 316L from vibration, and oxide layer formation on aluminium in salt water, while 316L exhibited yellowish discoloration under chloride exposure. Surface roughness trends revealed aluminium roughened in oil due to abrasive wear but smoothed in salt water through oxide formation and removal, whereas 316L consistently became smoother under both conditions due to lubrication and passive film stability. These mechanisms - abrasive wear, corrosion, and polishing can be encoded into digital twins for real-time degradation modelling. Recommendations include applying protective coatings, normalising 3D-printed parts, alloying with tungsten and nickel for corrosion resistance, and using CMM for nano-scale defect detection. Future work will consider hydrogen embrittlement risks in impellers operating in hydrogen-rich or humid environments, as hydrogen ingress can accelerate crack initiation and compromise fatigue life, making hydrogen compatibility a critical parameter for next-generation digital twin models. Although Industry 4.0 provides vast resources for predictive maintenance, integrating material science insights such as real-time surface defect prediction and phase transformations via IoT and digital twins remains an open challenge requiring significant research in digital engineering.

References

1. I. McKay, & A. Anbalagan, A FEA simulation study on impeller failures considering various materials. *Materials Today: Proceedings*, 80, 54–61 (2023).
2. Anbalagan, A., Kauffman, M., & Long, T. (2024, June). *Advancing Digital Twin Technology in Manufacturing: A Comprehensive Study on Data Capture and*

- Simulation of End Mills. In *International Manufacturing Science and Engineering Conference* (Vol. 88100, p. V001T02A010). American Society of Mechanical Engineers.
3. A. G. Frank, L. S. Dalenogare, & N. F. Ayala, Industry 4.0 technologies: Implementation patterns in manufacturing companies. *International Journal of Production Economics*, 210, 15–26 (2019). <https://doi.org/10.1016/j.ijpe.2019.01.004>
 4. Hughes, L., Dwivedi, Y. K., Rana, N. P., Williams, M. D., & Raghavan, V. (2022). Perspectives on the future of manufacturing within the industry 4.0 era. *Production Planning & Control*, 33(2-3), 138-158.
 5. D. I. Lee, & H. C. Lim, Erosion-corrosion damages of water-pump impeller. *International Journal of Automotive Technology*, 10(5), 629–634 (2009). <https://doi.org/10.1007/s12239-009-0074-5>
 6. A. Van Bennekom, F. Berndt, & M. N. Rassool, Pump impeller failures – A compendium of case studies. *Engineering Failure Analysis*, 8(2), 145–156 (2001). [https://doi.org/10.1016/S1350-6307\(99\)00044-8](https://doi.org/10.1016/S1350-6307(99)00044-8)
 7. K. Alexander, B. Donohue, T. Feese, G. Vanderlinden, & M. Kral, Failure analysis of an MVR (mechanical vapor recompressor) impeller. *Engineering Failure Analysis*, 17(6), 1345–1358 (2010). <https://doi.org/10.1016/j.engfailanal.2010.03.009>
 8. Z. W. Yu, X. L. Xu, J. Guo, & T. Cai, Fracture analysis of impeller blade of a locomotive draught-fan. *Engineering Failure Analysis*, 27, 16–29 (2013). <https://doi.org/10.1016/j.engfailanal.2012.12.004>
 9. R. Wei, X. Chen, Z. Ai, & Y. Jin, Experimental study and numerical simulation on the SSCC in FV520B stainless steel exposed to H₂S + Cl⁻ environment. *International Journal of Hydrogen Energy*, 43(18), 9059–9067 (2018). <https://doi.org/10.1016/j.ijhydene.2018.03.056>
 10. X. Zhang, W. Zhao, & Y. Xie, Fatigue failure analysis of semi-open impeller with mistuning considered. *Engineering Failure Analysis*, 95, 127–139 (2019). <https://doi.org/10.1016/j.engfailanal.2018.09.014>
 11. X. V. Wang, & L. Wang, Digital twin-based WEEE recycling, recovery and remanufacturing in the background of Industry 4.0. *International Journal of Production Research*, 57(12), 3892–3902 (2019). <https://doi.org/10.1080/00207543.2018.1497819>
 12. I. Castelo-Branco, F. Cruz-Jesus, & T. Oliveira, Assessing Industry 4.0 readiness in manufacturing: Evidence for the European Union. *Computers in Industry*, 107, 22–32 (2019). <https://doi.org/10.1016/j.compind.2019.01.007>
 13. D. Li, H. Tang, S. Wang, & C. Liu, A big data enabled load-balancing control for smart manufacturing of Industry 4.0. *Cluster Computing*, 20, 1855–1864 (2017). <https://doi.org/10.1007/s10586-017-0891-0>
 14. M. Ehrlich, L. Wisniewski, & J. Jasperneite, State of the art and future applications of industrial wireless sensor networks. In *Kommunikation und Bildverarbeitung in der Automation* (pp. 28–39). Springer (2018). https://doi.org/10.1007/978-3-662-55232-2_3
 15. J. H. Kim, A review of cyber-physical system research relevant to the emerging IT trends: Industry 4.0, IoT, big data, and cloud computing. *Journal of Industrial Integration and Management*, 2(3), 1750011 (2017). <https://doi.org/10.1142/S2424862217500117>

16. R. Y. Zhong, X. Xu, E. Klotz, & S. T. Newman, Intelligent manufacturing in the context of Industry 4.0: A review. *Engineering*, 3(5), 616–630 (2017). <https://doi.org/10.1016/J.ENG.2017.05.015>
17. E. Oztemel, & S. Gursev, Literature review of Industry 4.0 and related technologies. *Journal of Intelligent Manufacturing*, 31, 127–182 (2020). <https://doi.org/10.1007/s10845-018-1433-8>
18. F. Tao, Q. Qi, L. Wang, & A. Y. C. Nee, Digital twins and cyber–physical systems toward smart manufacturing and Industry 4.0: Correlation and comparison. *Engineering*, 5(4), 653–661 (2019). <https://doi.org/10.1016/j.eng.2019.01.014>
19. M. Saqlain, M. Piao, Y. Shim, & J. Y. Lee, Framework of an IoT-based industrial data management for smart manufacturing. *Journal of Sensor and Actuator Networks*, 8(2), 25 (2019). <https://doi.org/10.3390/jsan8020025>
20. J. Wan, B. Chen, M. Imran, F. Tao, D. Li, C. Liu, & S. Ahmad, Toward dynamic resources management for IoT-based manufacturing. *IEEE Communications Magazine*, 56(2), 52–59 (2018). <https://doi.org/10.1109/MCOM.2018.1700460>
21. Oliveira, M., Chauhan, S., Pereira, F., Felgueiras, C., & Carvalho, D. (2023). Blockchain protocols and edge computing targeting industry 5.0 needs. *Sensors*, 23(22), 9174.
22. Freitas, Luis, Marco Silva, Gabriel Vale, Camelia Avram, Helena Lopes, Filipe Pereira, Nuno Leal, and José Machado. "OPC UA and MQTT performance analysis within a unified namespace context." *Internet of Things* (2025): 101734.
23. Freitas, Luis, Filipe Pereira, Helena Lopes, Camelia Avram, Nuno Leal, Teresa Morgado, and José Machado. "OPC-UA vs. MQTT (UNS): Evaluating Alignment with RAMI4. 0 Through Literature Review." In *International Conference Innovation in Engineering*, pp. 434-445. Cham: Springer Nature Switzerland, 2025.
24. <https://nodered.org/> (Date Last Accessed: 12/10/2025)
25. Arduino. (n.d.). UNO R3. Arduino Documentation. Retrieved from <https://docs.arduino.cc/hardware/unos-rev3/>
26. <https://plm.sw.siemens.com/en-US/insights-hub/> (Date Last Accessed: 02/11/2025)
27. SparkFun. (n.d.). Piezo vibration sensor hookup guide. SparkFun Learn. Retrieved from <https://learn.sparkfun.com/tutorials/piezo-vibration-sensor-hookup-guide/all>